Bull. Mater. Sci., Vol. 34, No. 7, December 2011, pp. 1693–1698. © Indian Academy of Sciences.

Nitrates–melt synthesized $LiNi_{0.8}Co_{0.2}O_2$ and its performance as cathode in Li-ion cells

M SATHIYA, K HEMALATHA, K RAMESHA, A K SHUKLA[†] and A S PRAKASH*

CSIR – Central Electrochemical Research Institute – Chennai Unit, CSIR – Madras Complex, Chennai 600 113, India
[†]Solid State and Structural Chemistry Unit, Indian Institute of Science, Bangalore 560 012, India

MS received 28 March 2011; revised 6 May 2011

Abstract. Layered $LiNi_{0.8}Co_{0.2}O_2$ crystallizing in $R\bar{3}m$ space group is synthesized by decomposing the constituent metal–nitrate precursors. Oxidizing nature of metal nitrates stabilizes nickel in +3 oxidation state, enabling a high degree of cation ordering in the layered $LiNi_{0.8}Co_{0.2}O_2$. The powder sample characterized by XRD Rietveld refinement reveals < 2% Li–Ni site exchange in the layers. Scanning electron microscopic studies on the as-synthesized $LiNi_{0.8}Co_{0.2}O_2$ sample reflect well defined particles of cubic morphology with particle size ranging between 200 and 250 nm. Cyclic voltammograms suggest that $LiNi_{0.8}Co_{0.2}O_2$ undergoes phase transformation on first charge with resultant phase being completely reversible in subsequent cycles. The first-charge-cycle phase transition is further supported by impedance spectroscopy that shows substantial reduction in resistance during initial de-intercalation. Galvanostatic charge–discharge cycles reflect a first-discharge capacity of 184 mAh g^{-1} which is stabilized at 170 mAh g^{-1} over 50 cycles.

Keywords. Lithium batteries; intercalation compounds; electrochemical characterization; diffusion.

1. Introduction

Layered $LiCoO_2$ is extensively used as cathode material in commercial Li-ion batteries (Nagaura and Tozawa 1990). But the capacity of the $LiCoO_2$ cathode is limited to extraction of 0·5 Li because the Co^{4+}/Co^{3+} redox couple is pinned at the top of the O–2*p* band and any further removal of Li oxidizes O^{2-} ions at the surface into peroxide $(O_2)^{2-}$ ions evolving oxygen according to the reaction: $(O_2)^{2-} \leftrightarrow O^{2-} + 1/2O_2\uparrow$, causing safety concerns (Montoro *et al* 2000; Goodenough and Kim 2010). Solemn efforts have been extended to reduce the cost and toxicity of $LiCoO_2$ while improving its capacity and safety. These attempts have led to batteries with layered cathodes having little or substantially lesser cobalt. Among many such possible solid solutions of $LiMO_2$ (M = Co, Ni and Mn), $LiNi_{0.8}Co_{0.2}O_2$, $LiNi_{1/3}Mn_{1/3}Co_{1/3}O_2$ and $LiNi_{1/2}Mn_{1/2}O_2$ are most attractive (Delmas *et al* 1993; Saadoune and Delmas 1996; Wang *et al* 2000; Ohzuku and Makimura 2001; Makimura and Ozhuku 2003).

$LiNi_{0.8}Co_{0.2}O_2$, a nickel-rich phase of $LiNi_{1-x}Co_xO_2$ system, crystallizes in $R\bar{3}m$ space group with hexagonal ordering isostructural to $LiCoO_2$ and $LiNiO_2$ (Delmas *et al* 1993). Small amounts of cobalt in the framework of $LiNi_{1-x}Co_xO_2$ reduce Jahn–Teller distortion of Ni^{3+}-ions and help minimizing structural strain associated with distorted NiO_6 octahedra. This decreases the electrode resistance and helps sustaining high capacity of $LiNi_{1-x}Co_xO_2$. Besides, stronger Co–O bond helps stabilizing the structure during cycling with enhanced thermal stability of the material (Wang *et al* 2000). Accordingly, the solid solutions of $LiNi_{1-x}Co_xO_2$ exhibit a capacity value higher than $LiCoO_2$ and occlude the deficiencies of the end members (Delmas *et al* 1993; Saadoune and Delmas 1996; Wang *et al* 2000).

Important criteria for successful commercialization of cost-effective cathode materials is to prepare them in bulk by a simple synthetic route. Several methods, such as sol–gel route (Zhong *et al* 2006), co-precipitation (Wu and Yang 2005), reverse micro-emulsion (Lu and Wang 2003), rheological-phase synthesis (Wang *et al* 2007), spray pyrolysis (Wu *et al* 2006), have been used to synthesize layered $LiNi_{0.8}Co_{0.2}O_2$ with high homogeneity, perfect layered-structure, optimum particle-size and shape. But these methods are unattractive for bulk production as they involve multi-step processes. By contrast, the nitrates-melt-decomposition method reported (Sathiya *et al* 2009a, b) for the synthesis of $LiCoO_2$ and $LiNi_{1/3}Mn_{1/3}Co_{1/3}O_2$ is attractive for the preparation of other Li-ion cathode materials in bulk quantities as the method requires considerably lower temperatures and shorter durations in addition to the lower cost of the metal nitrates. Besides, the method yields a highly homogeneous product with improved electrochemical properties.

*Author for correspondence (prakash.as@gmail.com)

Mixed metal-nitrates melt at lower temperatures (~ 300°C) and form a homogeneous mixture that decomposes on further heating to give the final product. High homogeneity of the mixed-metal ions in the melt facilitates formation of pure compounds with perfectly-layered arrangement of atoms. In addition, the oxidizing nature of nitrates stabilizes nickel in Ni^{+3}-states preventing Ni from taking Li^+-sites in the structure. It is noteworthy that Ni^{2+} has ionic radius close to Li^+ and hence presence of Ni^{2+} facilitates cation mixing as has been observed in layered $LiNi_{0.8}Co_{0.2}O_2$ (Cho and Chung 2005).

This study reports the synthesis of layered $LiNi_{0.8}Co_{0.2}O_2$ by nitrates-melt-decomposition route and its attractive performance as Li-ion battery cathode.

2. Experimental

Powder sample of $LiNi_{0.8}Co_{0.2}O_2$ was prepared by heating the mixture of corresponding salts, viz. $LiNO_3$, $Ni(NO_3)_2 \cdot 6H_2O$ and $Co(NO_3)_2 \cdot 6H_2O$ at appropriate temperature followed by sintering. The molar ratios of the metal nitrates were taken such that Li : Ni : Co was 1·1 : 0.8 : 0·2. A 10% excess lithium, i.e. lithium-to-transition-metals ratio of 1·1 : 1, was taken to compensate for any lithium loss during calcination at higher temperatures. In a typical synthesis, 6·543 g of $LiNO_3$, 3·567 g of $Ni(NO_3)_2 \cdot 6H_2O$ and 0·8234 g of $Co(NO_3)_2 \cdot 6H_2O$ were taken in a 120 cm^3 alumina crucible and introduced into a cubical muffle furnace pre-heated to 400°C. The metal-nitrates melted and formed homogenized liquid which underwent decomposition. The furnace temperature was maintained at 400°C for 3 h to ensure complete decomposition of metal nitrates to yield partially formed product which was heated at 800°C for 3 h to obtain the final phase.

X-ray diffraction pattern for the sample was recorded using X'pert PRO-PANalytical diffractometer using CuK_α radiation. The crystal structure, lattice parameters and extent of Li/Ni cation mixing in the sample were determined by Rietveld refinement of powder X-ray diffraction data using general structure analysis system (GSAS) code (Larson and van Dreele 2000; Toby 2001). The morphology and particle size of the powder sample were investigated with a scanning electron microscope (HITACHI Model S-3000H). The electrode for electrochemical studies was prepared by mixing 85% active material and 15% SP carbon (Timcal, Belgium) as conducting additive. Swagelok™ type cells were assembled and sealed in an argon-filled glove box with lithium foil as the anode and 1 M $LiPF_6$ dissolved in EC/DMC (1 : 1 by volume) as the electrolyte. The cells thus fabricated were cycled in potentiostatic and galvanostatic modes in the voltage range between 3 and 4·3 V vs lithium using VMP3Z Biologica multi-channel potentiostat/galvanostat. Impedance measurements were carried out using three electrode assemblies with lithium as reference and counter electrode. The impedance spectra were recorded at various state-of-charge values of the cell during galvanostatic cycling at 0·2C rate in the frequency range between 400 kHz and 2 mHz. The data were analysed using ZSimpWin software with complex nonlinear-least-squares fit.

3. Results and discussion

Structural analysis of $LiNi_{0.8}Co_{0.2}O_2$ sample synthesized by nitrates-melt-decomposition route is carried out using Rietveld refinement of powder X-ray diffraction (XRD) pattern. The XRD Rietveld-fits for observed, calculated and difference patterns are shown in figure 1. $LiNiO_2$ structure with $R\bar{3}m$ space group is used as initial structural model wherein Ni, Li and O are fixed at 3*a*, 3*b* and 6*c* sites, respectively. Refinement is carried out by fixing Co at the 3*a* sites while allowing Li and Ni to disorder between 3*a* and 3*b* sites. As seen in figure 1, the refinement converges with a good fit between the experimental and calculated patterns. The crystallographic parameters obtained using refined powder XRD pattern are presented in table 1. Li/Ni disorder observed here is only 1·8% and indicates a highly-ordered arrangement of metal cations in the sample. The low-cation mixing (< 2%) observed here is attributed to the stabilization of high concentration of Ni^{+3} in the sample owing to the oxidizing nature of nitrate flux used in the synthesis. Formation of perfectly-ordered-layered structure is obvious from clear splitting of the (006)/(102), (108)/(110) peaks shown as inset in figure 1. Furthermore, the intensity ratio $I_{(003)}/I_{(104)}$ is found to be 1·48 which is higher than that for disordered sample indicating high cation ordering (Oh *et al* 2005). The *R*-factor, described as the intensity ratio $I_{(1\,0\,2)} + I_{(0\,0\,6)}/I_{(1\,0\,1)}$, is also used as a measure for degree of cation mixing (Reimers *et al* 1993). The *R*-factor calculated

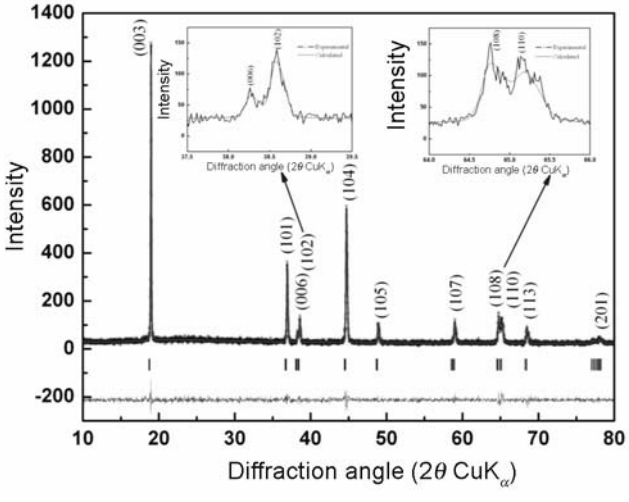

Figure 1. Powder XRD Rietveld fit for $LiNi_{0.8}Co_{0.2}O_2$ derived from nitrates-melt decomposition.

Table 1. Refined crystallographic parameters for nitrate-melt synthesized $LiNi_{0·8}Co_{0·2}O_2$.

Atom	*X*	*Y*	*Z*	Occupancy
Li 1	0·0	0·0	0·5	0·981 (6)
Li 2	0·0	0·0	0·0	0·018 (4)
Ni 1	0·0	0·0	0·0	0·781 (6)
Ni 2	0·0	0·0	0·5	0·018 (4)
Co 1	0·0	0·0	0·0	0·200 (0)
O 1	0·0	0·0	0·2583	1·000 (0)

Lattice parameters: $a = b = 2·868(1)$ Å, $c = 14·173(1)$ Å; space group: $R\bar{3}m$, $c/a = 4·942$, Li/Ni disorder is $1·80(1)\chi^2 = 0·8259$.

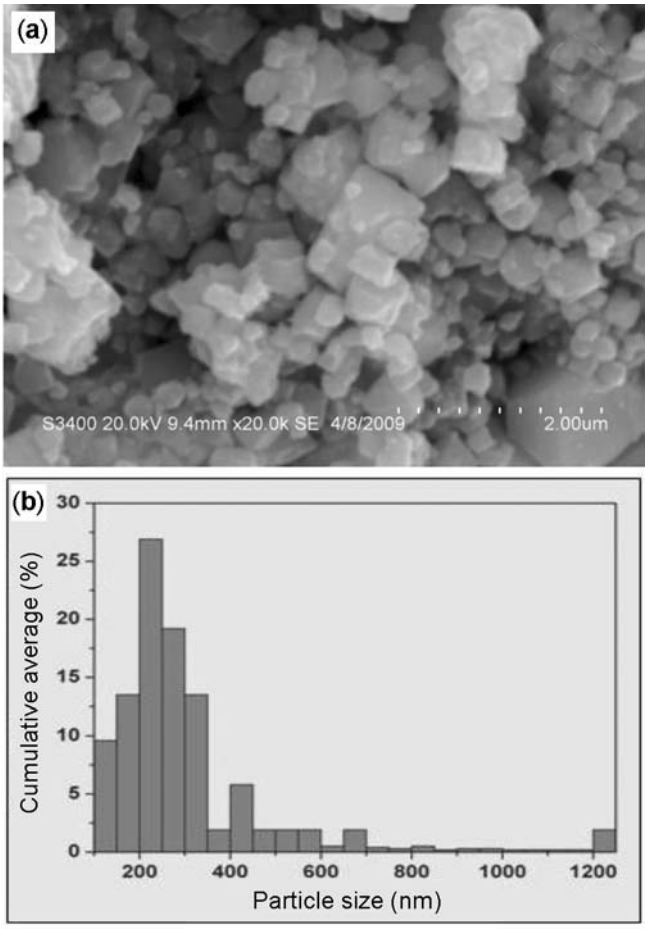

Figure 2. (**a**) Scanning electron micrograph for $LiNi_{0.8}Co_{0.2}O_2$ and (**b**) histogram shows particle-size distribution.

from the intensities of the corresponding peaks is as low as 0·4658 that also suggests high hexagonal-ordering in the sample (Reimers *et al* 1993).

Particle-size distribution and morphological studies are carried out using scanning electron microscopy. The representative SEM image for $LiNi_{0·8}Co_{0·2}O_2$ synthesized by nitrate-melts decomposition is depicted in figure 2. The micrograph illustrates well developed and nearly-cubic crystallites with a narrow size-distribution typically ranging between 100 and 350 nm. The histogram for particle-size distribution derived from the SEM image is shown in figure 2(b). It is seen from the histogram that the maximum percentage of particles have size distribution between 200 and 250 nm.

Figure 3 shows the cyclic voltammogram (CV) for $LiNi_{0·8}Co_{0·2}O_2$ vs Li in the voltage range between 3 and 4·3 V with a scan rate of 0·1 mV s^{-1}. During the first cycle, a peak at 4·1 V is observed which is associated with the co-existence of two hexagonal phases, H_1 and H_2, related to $Li_{1-x}Ni_{0·8}Co_{0·2}O_2$ (Ronci *et al* 2001; Gross *et al* 2005). The subsequent cycles differ from the first cycle suggesting the transformation of initial phase to a new phase as reported by Gross *et al* (2005). Subsequent reduction causes a monotonic increase in current response with a maximum at 3·6 V. $Li_xNi_{0·8}Co_{0·2}O_2$ is known to exhibit phase transitions on Li de-intercalation. Song *et al* (2008) reported that $Li_xNi_{0.8}Co_{0.2}O_2$ adopts monoclinic structure for $0·5 \le x \le 0·7$ compositions while it crystallizes in rhombohedral structure for $x \ge 0·8$ and $x \le 0·4$ compositions. Accordingly, the peaks observed here at 3·9 and 3·6 V are attributed to the coexistence of rhombohedral/monoclinic and monoclinic/rhombohedral phases, respectively.

Figure 4 shows the voltage vs composition curve derived from galvanostatic charge/discharge experiments for $LiNi_{0·8}Co_{0·2}O_2$/Li cell in the voltage range between 3 and 4·3 V at 0·2C rate. About 0·1 Li, corresponding to a capacity of 20 mAh g^{-1}, is irreversible during the first cycle. This irreversibility could be attributed to the transformation of initial phase to a new Li-deficient phase together with formation of SEI during initial charge cycle. The irreversible loss during second cycle is small and the material exhibits good capacity retention during subsequent cycles as shown in figure 4(b). The sample shows initial charge/discharge capacity of 204/185 mAh g^{-1}. About 90% of initial capacity is retained even after 50 cycles. Low polarization observed between the charge and discharge curves suggests smooth accommodation of lithium during intercalation/de-intercalation processes with good inter-particle contact.

To further comprehend the electrochemical data presented in figures 3 and 4, impedance measurements are

carried out on $LiNi_{0.8}Co_{0.2}O_2$/Li cells in three-electrode assembly configuration with lithium counter and reference. The impedance data are collected at varying state-of-charge values during galvanostatic cycling between 3 and 4·3 V at 0·2C rate. Impedance spectra for as fabricated cells along with impedance spectra for the cell after de-intercalation of 0·1 Li are depicted in figure 5. It is seen that impedance of the fresh cell is high and hence the spectrum is not fully developed in the measured frequency region. Even on de-intercalation of 0·1 Li, corresponding to the composition $Li_{0.9}Ni_{0.8}Co_{0.2}O_2$, a substantial decrease in the resistivity is observed. It is known that $LiNi_{0.8}Co_{0.2}O_2$ undergoes transition from semiconductor to metallic state at the initial stages of de-intercalation process (Nobili *et al* 2001). This transition is supposedly responsible for the reduction in resistance on de-intercalation of 0·1 lithium.

Variation in impedance parameters during different levels of intercalation/de-intercalation is further probed for one full charge and discharge cycle. Figure 6 shows the Nyquist plots for $LiNi_{0.8}Co_{0.2}O_2$/Li cell during lithium de-intercalation (a–e) and lithium intercalation (f–j) at different potentials. Experimental values are shown as points and the respective fit using equivalent circuit model is depicted by solid line. The spectrum reveals two semicircular regions and a slopping line at a constant angle. The semicircle at high-frequency region (> 50 Hz) is generally attributed to the Li-ion migration through the surface passive film, viz. solid electrolyte interface (SEI), present on the cathode active surface. The semicircle at middle frequency (40–1 Hz) is assigned to charge-transfer through the cathode/electrolyte interface, and the low-frequency line (lower mHz) to lithium-ion diffusion through bulk of the cathode. Hence, the impedance spectrum shown here is fitted with Frumkin–Melik–Gaykazyan model (Levi and Aurbach 1997) where the equivalent circuit comprises electrolyte resistance, R_e, in series with two RC networks in conjunction with Z_{FLW} element

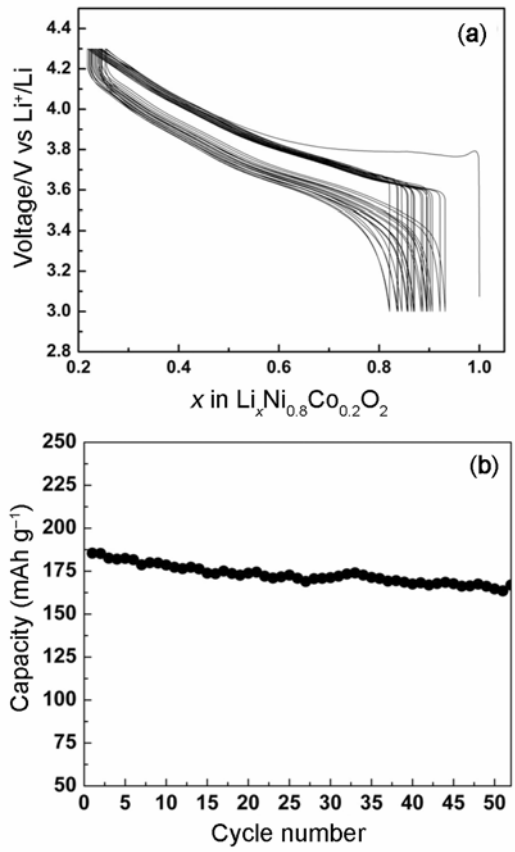

Figure 4. (**a**) Voltage vs composition data derived from galvanostatic charge/discharge experiments on $LiNi_{0.8}Co_{0.2}O_2$/Li cell in voltage range between 3 and 4·3 V at 0·2C rate and (**b**) discharge capacity vs cycle number.

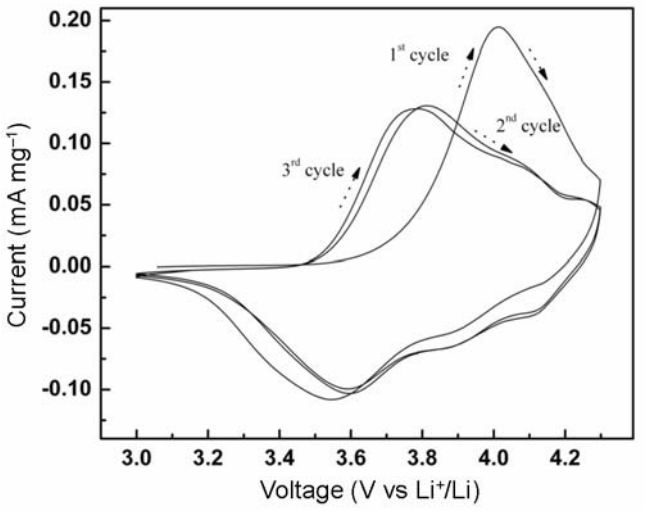

Figure 3. Cyclic voltammograms for $LiNi_{0.8}Co_{0.2}O_2$ vs Li cells in voltage range 3–4·3 V with a scan rate of 0·1 mV/s.

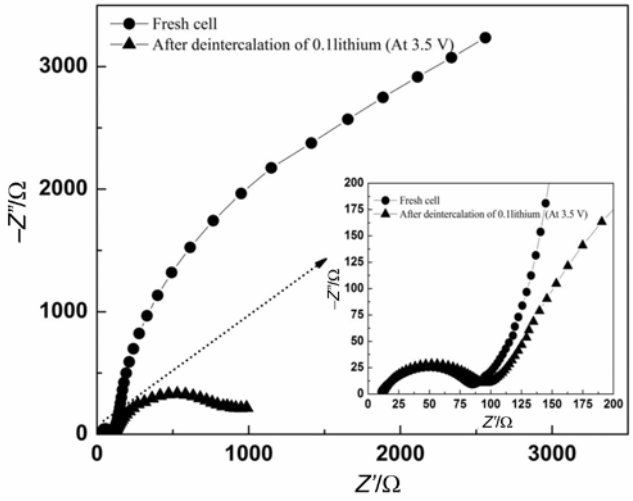

Figure 5. Impedance spectra for fresh cell together with that after de-intercalation of 0·1 Li in frequency range between 400 kHz and 2 mHz in galvanostatic mode. Inset shows magnified high-frequency region.

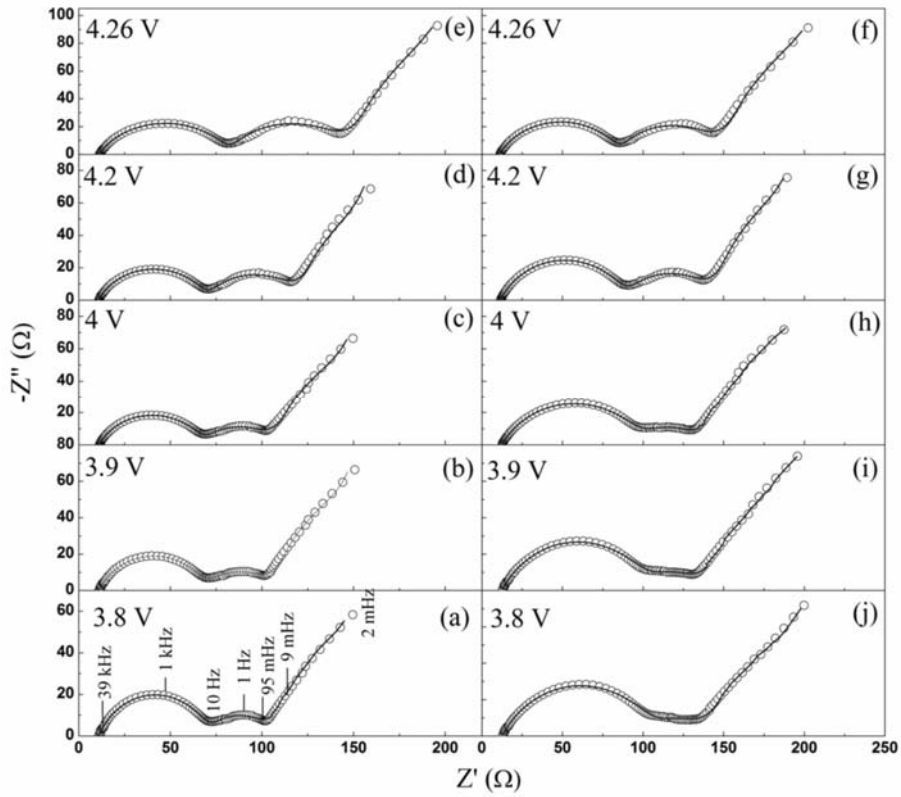

Figure 6. Nyquist plots for $LiNi_{0·8}Co_{0·2}O_2$ half cells during de-intercalation (a–e) and intercalation (f–j) of lithium.

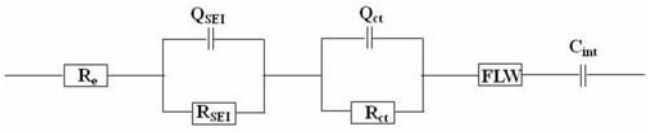

Figure 7. Equivalent circuit model used for fitting impedance spectrum. R_e is the ohmic resistance due to electrolyte, R_{SEI} and R_{ct} are total resistance associated with solid electrolyte interface and charge transfer, respectively. Q_{SEI} and Q_{ct} are constant phase elements for SEI and charge transfer. FLW is finite-length Warburg and C_{int} represents intercalative capacitance.

followed by intercalative capacitance. The model equivalent circuit is shown in figure 7. The constant-phase element, Q ($Q = 1/jY\omega^n$), is used instead of a capacitor to explain the depressed semicircle. In intercalation compounds, solid-state diffusion is normally associated with accumulation of charge on the surface resulting in capacitive behaviour at low frequencies (Mohamedi *et al* 2001). Accordingly, finite length Warburg element (Z_{FLW}) in series with C_{int} is used in the circuit to represent diffusion and accumulation of lithium at the $LiNi_{0·8}Co_{0·2}O_2$ electrode (Levi *et al* 2000).

Figure 8 shows the variation in resistive and capacitive components during lithium de-intercalation (a–c) and lithium intercalation (d–f). Resistance of SEI film, denoted as R_{SEI} (a, d), and cathodic resistance, denoted as R_{ct} (b, e), are derived from equivalent circuit fit values. From the data, it is seen that resistance values associated with SEI film during charge changes only nominally due to the initial SEI formation on the cathode active surface in contact with electrolyte. During the discharge process, resistance due to SEI gradually increases with higher increase in the potential region between 3·5 and 3·8 V. This increase is linked to creation of larger active surface during first discharge process (Zhang *et al* 2002). The change in cathodic resistance during charge–discharge shown in figures 8(b) and (e) agree well with the CV data. It is noteworthy that cathodic resistance, R_c, is lower for peak potentials in CV while it is comparatively higher at the other points. By contrast, intercalative capacitance denoted as C_{int} in figures 8(c) and (f) is high at the observed peak potentials in CV. Intercalative capacitance, C_{int}, is calculated from:

$$C_{int} = -1/\omega Z''_{\omega \to 0},$$

where $\omega = 2\pi\gamma$ with γ as the linear frequency (Levi *et al* 2000) and C_{int} is the capacitance due to accumulation of lithium into the host material and is analogous to pseudo-capacitance. Amount of accumulated lithium depends on the available lattice sites in the host material that in turn depends on the electrode potential. Since the amount of lattice positions available in the host material is higher at peak potentials, C_{int} also happens to be high at these potentials (Levi and Aurbach 1999).

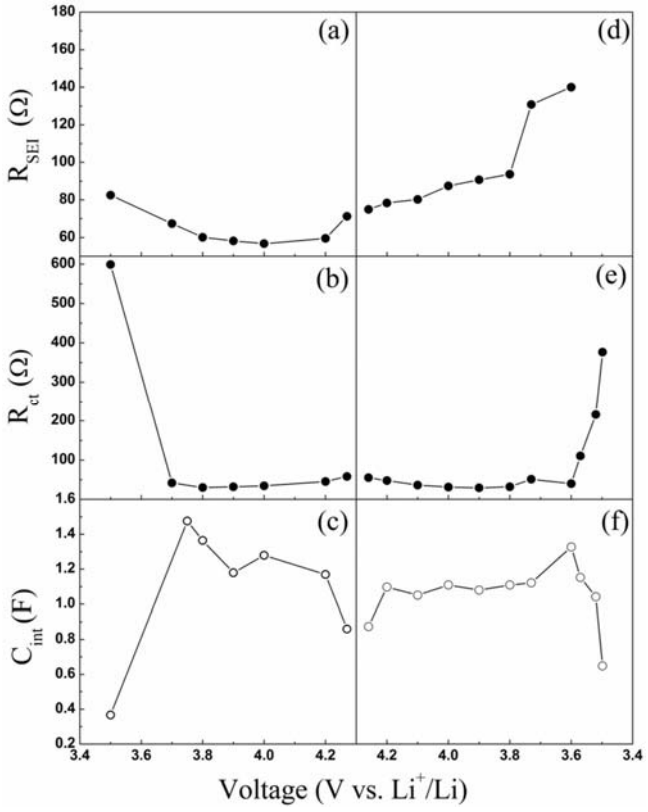

Figure 8. Variation in resistive and capacitive components for cell during lithium de-intercalation (a–c) and intercalation (d–f). Resistance due to SEI layer is denoted as R_{SEI} (a, d) and charge transfer resistance as R_{ct} (b, e).

4. Conclusions

$LiNi_{0.8}Co_{0.2}O_2$ having ordered-layered structure and $R\bar{3}m$ space group with $<2\%$ cation mixing is synthesized by nitrates-melt-decomposition route. The process yields highly homogeneous powders having near-cubic morphology with maximum particle-size distribution between 200 and 250 nm. The cyclic voltammograms reveal that $LiNi_{0.8}Co_{0.2}O_2$ undergoes a phase transformation during first cycle. In the subsequent cycles, the new phase undergoes a series of phase transformations from rhombohedral to monoclinic and finally to rhombohedral phase that are completely reversible. The impedance data on $LiNi_{0.8}Co_{0.2}O_2$ electrodes indicate that the phase transition observed during the first cycle is linked to occurrence of semiconductor–metal transition on de-intercalation of 0·1 Li. The galvanostatic charge–discharge studies reflect improved electrochemical performance of nitrates-melt synthesized $LiNi_{0.8}Co_{0.2}O_2$ with a stable capacity of 175 mAh g^{-1} during prolonged cycling.

Acknowledgements

One of the authors (MS) thanks CSIR, New Delhi, for a Senior Research Fellowship. Financial support from the EMPOWER Scheme (DUO1OLP-0062) of the Council of Scientific and Industrial Research, New Delhi, is gratefully acknowledged.

References

Cho T H and Chung H -T 2005 *J. Appl. Electrochem.* **35** 1033
Delmas C, Saadoune I and Rougier A 1993 *J. Power Sources* **44** 595
Gross T, Buhrmester Th, Bramnik K G, Bramnik N N, Nikolowski K, Baehtz C, Ehrenberg H and Fuess H 2005 *Solid State Ionics* **176** 1193
Goodenough J B and Kim Y 2010 *Chem. Mater.* **22** 587
Larson A C and Van Dreele R B 2000 Los Alamos National Laboratory Report No. LAUR **86** 748
Levi M D and Aurbach D 1997 *J. Phys. Chem.* **B101** 4630
Levi M D and Aurbach D 1999 *Electrochim. Acta* **45** 167
Levi M D, Gamolsky K, Aurbach D, Heider U and Oesten R 2000 *Eletrochim. Acta* **45** 1781
Lu C -H and Wang H-C 2003 *J. Mater. Chem.* **13** 428
Makimura Y and Ohzuku T 2003 *J. Power Sources* **119–121** 156
Mohamedi M, Takahashi D, Uchiyama T, Itoh T, Nishizawa M and Uchida I 2001 *J. Power Sources* **93** 93
Montoro L A, Abbate M and Rosolen J M 2000 *Electrochem. Solid-State Lett.* **3** 410
Nagaura T and Tozawa K 1990 *Prog. Batt. Sol. Cells* **9** 209
Nobili F, Croce C, Scrosati B and Marassi R 2001 *Chem. Mater.* **13** 1642
Oh S H, Jeong W T, Cho W II, Cho B W and Woo K 2005 *J. Power Sources* **140** 145
Ohzuku T and Makimura Y 2001 *Chem. Lett.* **30** 642
Reimers J N, Rossen E, Jones C D and Dahn J R 1993 *Solid State Ionics* **61** 335
Ronci F, Scrosati B, Albertini V R and Perfetti P 2001 *J. Phys. Chem.* **B105** 754
Saadoune I and Delmas C 1996 *J. Mater. Chem.* **6** 193
Sathiya M, Prakash A S, Ramesha K and Shukla A K 2009a *Materials* **2** 857
Sathiya M, Prakash A S, Ramesha K and Shukla A K 2009b *Mater. Res. Bull.* **44** 1990
Song M K, Hong S D and No K T 2008 *J. Phys. Chem. Solids* **69** 1249
Toby B H 2001 *J. Appl. Crystallogr.* **34** 210
Wang C, Ma X, Zhou L, Cheng J, Sun J and Zhou Y 2007 *Eletrochim. Acta* **52** 3022Wang G X, Horvat J, Bradhurst D H, Liu H K and Dou S X 2000 *J. Power Sources* **85** 279
Wu H M, Tu J P, Chen X T, Yuan Y F, Li Y, Zhao X B and Cao G S 2006 *J. Power Sources* **159** 291
Wu S -H and Yang C -W 2005 *J. Power Sources* **146** 270
Zhang S S, Xu K and Jow T R 2002 *J. Electrochem. Soc.* **149** A1521
Zhong Y D, Zhao X B, Cao G S, Tu J P and Zhu T J 2006 *J. Alloys Compd.* **420** 298